Monthly Notices of the ROYAL ASTRONOMICAL SOCIETY

MNRAS **460,** 3772–3783 (2016) doi:10.1093/mnras/stw1247
Advance Access publication 2016 May 24

Alignments between galaxies, satellite systems and haloes

Shi Shao,[1,2]★ Marius Cautun,[2]★ Carlos S. Frenk,[2] Liang Gao,[1,2] Robert A. Crain,[3] Matthieu Schaller,[2] Joop Schaye[4] and Tom Theuns[2]

[1]*National Astronomical Observatories, The Partner Group of Max Planck Institute for Astrophysics, Chinese Academy of Sciences, Beijing 100012, China*
[2]*Institute for Computational Cosmology, Department of Physics, Durham University, South Road, Durham DH1 3LE, UK*
[3]*Astrophysics Research Institute, Liverpool John Moores University, IC2, 146 Brownlow Hill, Liverpool L3 5RF, UK*
[4]*Leiden Observatory, Leiden University, PO Box 9513, NL-2300 RA Leiden, the Netherlands*

Accepted 2016 May 19. Received 2016 May 19; in original form 2016 May 4

ABSTRACT

The spatial distribution of the satellite populations of the Milky Way and Andromeda are puzzling in that they are nearly perpendicular to the discs of their central galaxies. To understand the origin of such configurations we study the alignment of the central galaxy, satellite system and dark matter halo in the largest of the 'Evolution and Assembly of GaLaxies and their Environments' (EAGLE) simulation. We find that centrals and their satellite systems tend to be well aligned with their haloes, with a median misalignment angle of 33° in both cases. While the centrals are better aligned with the inner 10 kpc halo, the satellite systems are better aligned with the entire halo indicating that satellites preferentially trace the outer halo. The central–satellite alignment is weak (median misalignment angle of 52°) and we find that around 20 per cent of systems have a misalignment angle larger than 78°, which is the value for the Milky Way. The central–satellite alignment is a consequence of the tendency of both components to align with the dark matter halo. As a consequence, when the central is parallel to the satellite system, it also tends to be parallel to the halo. In contrast, if the central is perpendicular to the satellite system, as in the case of the Milky Way and Andromeda, then the central–halo alignment is much weaker. Dispersion-dominated (spheroidal) centrals have a stronger alignment with both their halo and their satellites than rotation-dominated (disc) centrals. We also found that the halo, the central galaxy and the satellite system tend to be aligned with the surrounding large-scale distribution of matter, with the halo being the better aligned of the three.

Key words: methods: numerical – galaxies: haloes – galaxies: kinematics and dynamics.

1 INTRODUCTION

The distribution of galactic satellites is highly inhomogeneous and anisotropic, as can be easily recognized from observations of the Local Group (LG). Most of the Milky Way (MW) satellites define a tight plane (Kunkel & Demers 1976; Lynden-Bell 1976, 1982; Kroupa, Theis & Boily 2005) that shows some degree of coherent rotation (Metz, Kroupa & Libeskind 2008; Pawlowski, Kroupa & Jerjen 2013). Even more puzzling is the orientation of this satellite plane which is almost perpendicular to the MW disc. The satellites of Andromeda (M31) are distributed mostly along two planar, nearly parallel structures that are offset from each other (Conn et al. 2013; Ibata et al. 2013; Shaya & Tully 2013). Such planes of satellites are common outside the LG too (e.g. the Centaurus A Group; Tully et al. 2015) with their characteristic signature detected in large stacked samples of external galaxies (Cautun et al. 2015a).

Within the standard Λ cold dark matter (ΛCDM) model, the anisotropic distribution of satellites is a manifestation of the preferential direction of accretion on to haloes (e.g. Aubert, Pichon & Colombi 2004; Knebe et al. 2004; Libeskind et al. 2005; Zentner et al. 2005; Li & Helmi 2008; Deason et al. 2011; Wang et al. 2014; Shi, Wang & Mo 2015). The flattened distributions of satellites can arise from the infall of satellites along the spine of filaments (Libeskind et al. 2005; Buck, Macciò & Dutton 2015) and that can also lead to a significant population of corotating satellites (Libeskind et al. 2009; Lovell et al. 2011; Cautun et al. 2015a). Despite ΛCDM predicting the existence of satellite planes, initial studies emphasized a perceived discrepancy with observations, with the MW and M31 satellite planes claimed to be thinner and to show a larger degree of coherent rotation than their ΛCDM counterparts (e.g. Pawlowski et al. 2012; Ibata et al. 2014). However, Cautun

★E-mail: shaoshi@bao.ac.cn (SS); m.c.cautun@durham.ac.uk (MC)

et al. (2015b) recently pointed out that this conclusion was based on a misinterpretation of the diversity of satellite planes (see also Buck, Dutton & Macciò 2016), since the characteristics of each plane (e.g. thickness, radial extent) vary strongly from halo to halo. In fact, the very diversity of satellite planes is a manifestation of the varied formation and evolution history of the host halo (e.g. see Buck et al. 2015; Smith et al. 2016).

In this paper, we investigate the information encoded in the preferential direction of the spatial distributions of satellites, focusing on the alignment of satellite planes with the direction of the central galaxies and host haloes. Within the ΛCDM cosmological model, dark matter (DM), gas and satellites are accreted preferentially along filaments suggesting that these various subsystems should be aligned to some extent (Libeskind et al. 2005, 2011, 2014). Most studies have focused on two aspects of these correlations. First, hydrodynamical simulations show that the central galaxy has a typical misalignment angle of $\approx 30^\circ$ with the DM halo, with an even stronger alignment for spheroids (e.g. Bett et al. 2010; Deason et al. 2011; Sales et al. 2012; Tenneti et al. 2014; Velliscig et al. 2015a). Secondly, both observations and simulations show that individual satellites are preferentially aligned along the major axis of the central galaxy, with the strongest alignment occurring between red satellites and red centrals (e.g. Brainerd 2005; Yang et al. 2006; Agustsson & Brainerd 2010; Nierenberg et al. 2012; Dong et al. 2014; Tenneti et al. 2014; Velliscig et al. 2015b). However, the alignment of the whole distribution of satellites with the central galaxy and with the DM halo, which is the focus of this study, has been largely overlooked (although see Libeskind et al. 2007, 2009; Deason et al. 2011), despite its importance for interpreting the LG observations. The satellite systems of both the MW and M31 are roughly perpendicular to the disc of their respective centrals and are thus difficult to reconcile with the expectation of the filamentary accretion hypothesis. To address this puzzle we will determine the prevalence of such perpendicular configurations and study their implications.

Our study makes use of the hydrodynamical simulations run as part of the Evolution and Assembly of GaLaxies and their Environments (EAGLE) project (Crain et al. 2015; Schaye et al. 2015). EAGLE implements the main physical processes that determine the formation and evolution of galaxies, incorporating the baryonic processes that affect the galaxy and halo shapes as well as the orbits of satellite galaxies. This simulation was used by Velliscig et al. (2015a) to study the alignments of the distributions of stars, hot gas and DM. They found that, while galaxies are well aligned with the local distribution of DM, they can have large misalignments with the entire halo. In a separate study, Velliscig et al. (2015b) used the same simulation to measure that the strength of the galaxy–galaxy alignment is a strongly decreasing function of the distance between the two objects (see also Welker et al. 2015). By contrast, our study focuses on the alignment of satellite systems and on its interplay with the central galaxy, the host halo and the surrounding distribution of matter.

The paper is organized as follows. Section 2 reviews the EAGLE simulation and describes our sample selection; Section 3 presents our main results; Section 4 discusses the implications of our findings; we conclude with a short summary in Section 5.

2 SIMULATION AND METHODS

We make use of the main cosmological hydrodynamical simulation (labelled Ref-L0100N1504) performed as part of the EAGLE project (Crain et al. 2015; Schaye et al. 2015). EAGLE assumes a *Planck* cosmology (Planck Collaboration XVI 2014) with cosmological parameters: $\Omega_\mathrm{m} = 0.307$, $\Omega_\mathrm{b} = 0.04825$, $\Omega_\Lambda = 0.693$, $h = 0.6777$, $\sigma_8 = 0.8288$ and $n_\mathrm{s} = 0.9611$. The simulation is of a periodic cube of 100 Mpc side length and follows the evolution 1504^3 DM and an initially equal number of baryonic particles. The DM particles have a mass of $9.7 \times 10^6\,\mathrm{M}_\odot$, while the gas particles have an initial mass of $1.8 \times 10^6\,\mathrm{M}_\odot$.

The simulation was performed using a version of the GADGET code (Springel 2005) which has been modified to include state-of-the-art smoothed particle hydrodynamics methods (Hopkins 2013; Schaller et al. 2015; Dalla Vecchia, in preparation). The baryonic physics implementation includes element-by-element cooling using the Wiersma, Schaye & Smith (2009a) prescription in the presence of a Haardt & Madau (2001) ultraviolet (UV) and X-ray background, stochastic star formation with a metallicity-dependent threshold (Schaye 2004) and a star formation rate that depends explicitly on pressure (Schaye & Dalla Vecchia 2008), thermal energy feedback associated with star formation (Dalla Vecchia & Schaye 2012) and the injection of hydrogen, helium and metals into the interstellar medium from supernovae and stellar mass loss (Wiersma et al. 2009b). Star particles are treated as single stellar populations with a Chabrier (2003) initial mass function. Supermassive black holes grow through mergers and accretion of low angular momentum material (Springel, Di Matteo & Hernquist 2005; Rosas-Guevara et al. 2015; Schaye et al. 2015) and the resulting active galactic nuclei (AGN) inject thermal energy into the surrounding gas (Booth & Schaye 2009; Dalla Vecchia & Schaye 2012). These subgrid models were calibrated to reproduce the present day stellar mass function and galaxy sizes, as well as the relation between galaxy stellar masses and supermassive black hole masses (Crain et al. 2015; Schaye et al. 2015). See Schaye et al. (2015) for a more detailed description of the baryonic processes implemented in EAGLE.

Haloes are identified using the friends-of-friends (FOF) algorithm with a linking length of 0.2 times the mean particle separation (Davis et al. 1985). Gravitationally bound substructures are identified using the SUBFIND code (Springel, Yoshida & White 2001; Dolag et al. 2009) applied to the full matter distribution (DM, gas and stars) associated with each FOF halo. The subhalo that contains the particle with the lowest gravitational energy is classified as the main halo and its stellar distribution as the central galaxy. The main haloes are characterized by the mass, M_{200}, and radius, R_{200}, that define an enclosed spherical overdensity of 200 times the critical density. The remaining subhaloes are classified as satellite galaxies. The position of each galaxy, for both centrals and satellites, is given by the particle that has the lowest gravitational potential energy.

2.1 Sample selection

To identify systems similar to the MW and M31, we start by selecting the 3209 haloes with mass $M_{200} \in [0.3, 3] \times 10^{12}\,\mathrm{M}_\odot$. The wide mass range is motivated by the large uncertainties in the mass of the MW (e.g. Fardal et al. 2013; Cautun et al. 2014; Piffl et al. 2014; Wang et al. 2015; Han et al. 2016) and the need to have a large sample of such systems. We require that any such halo be isolated and not overlap with more massive companions. Thus, we exclude all central galaxies that have a neighbour within 600 kpc that has a stellar mass larger than half their mass. We also restrict our selection to haloes that, like the MW, have at least 11 luminous satellites within a distance of 300 kpc from the central galaxy. A luminous satellite consists of a DM subhalo with at least one star particle. We obtain 1080 host haloes that satisfy all three selection criteria.

The sample has a median halo mass, $M_{200} \sim 1.2 \times 10^{12}\,\mathrm{M}_{\odot}$, and a median number of 15 luminous satellites per halo. The typical total mass of a luminous satellite is $M_{\rm tot} \sim 1 \times 10^{9}\,\mathrm{M}_{\odot}$, which corresponds to ∼100 DM particles (see Appendix A for the halo and satellite mass functions). Fig. 1 illustrates the distribution of stars and satellites in five haloes found in our sample. These systems, which we will discuss in detail in Section 3, were selected to have satellite system that are almost perpendicular to the central galaxy, similar to the configuration observed around the MW.

2.2 Shape definition

We compute the shape of the various galactic subsystems (e.g. halo, central galaxy, satellite population) using the moment of inertia tensor,[1]

$$I_{ij} \equiv \sum_{k=1}^{N} m_k x_{k,i} x_{k,j}, \tag{1}$$

where N is the number of particles that belong to the structure of interest, $x_{k,i}$ denotes the ith component ($i = 1, 2, 3$) of the position vector of particle k with respect to the halo centre and m_k denotes the mass of that particle. In the case of the halo, the sum is over all DM particles within R_{200}, while for the central galaxy the sum is over all the star particles within 10 kpc from the centre (which is approximately twice the average value of the half stellar mass radius in our sample). For the satellite system, the sum is over all the luminous satellites within 300 kpc of the centre, with each satellite being assigned a constant and equal mass, $m_k = 1$. We weight all the satellites equally to compare more closely to observations, where the satellite masses are highly uncertain, and to use the same approach as previous works which have studied planes of satellite galaxies (e.g. Libeskind et al. 2005, 2007; Pawlowski & Kroupa 2013; Wang, Frenk & Cooper 2013).

The shape and the orientation are determined by the eigenvalues, λ_i ($\lambda_1 \geq \lambda_2 \geq \lambda_3$), and the eigenvectors, $\hat{\boldsymbol{e}}_i$, of the inertia tensor. The major, intermediate and minor axes of the corresponding ellipsoid are given by $a = \sqrt{\lambda_1}$, $b = \sqrt{\lambda_2}$ and $c = \sqrt{\lambda_3}$, respectively. The computation of the inertia tensor using a spherical region biases the shape towards higher sphericity, but this has little effect on the orientation of the principal axes, which is the focus of our study (Frenk et al. 1988; Bailin & Steinmetz 2005).

2.3 The misalignment angle

We are interested in the degree of alignment between the galactic subsystems, which we will quantify in terms of a misalignment angle, θ. For example, the misalignment angle between the central galaxy and its parent halo is defined as

$$\theta_{\rm C-H} = \arccos(|\hat{\boldsymbol{e}}_3^{\rm C} \cdot \hat{\boldsymbol{e}}_3^{\rm H}|), \tag{2}$$

where $\hat{\boldsymbol{e}}_3^{\rm C}$ and $\hat{\boldsymbol{e}}_3^{\rm H}$ are the minor axes of the central galaxy and the halo, respectively. Note that we take the absolute value of the dot product because the eigenvectors determine only an orientation and do not have a direction assigned to them. The misalignment angles between the satellite plane and the halo, $\theta_{\rm S-H}$, and between the central galaxy and the satellite plane, $\theta_{\rm C-S}$, are computed similarly.

[1] Strictly speaking, I_{ij}, is not the moment of inertia tensor (see e.g. Bett et al. 2007), but we follow the common practice in this subject and adopt this nomenclature.

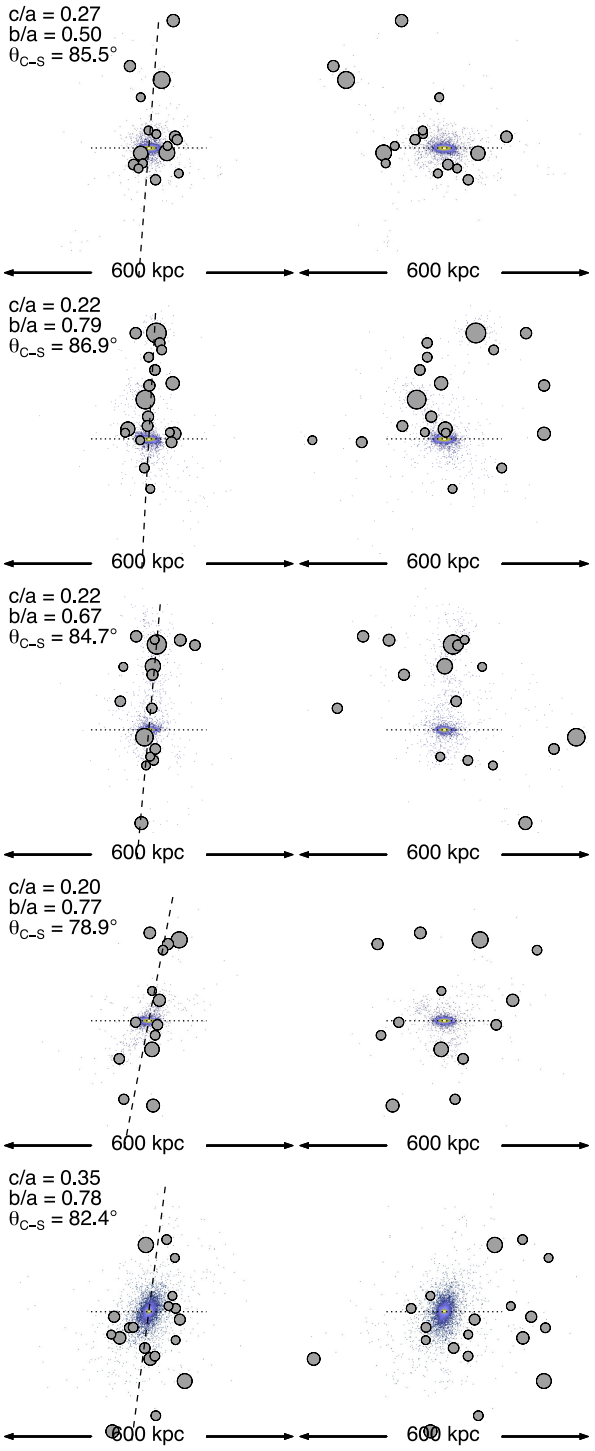

Figure 1. Examples of galactic systems that have planar satellite distributions that are almost perpendicular to the central galaxy. Each row shows a different system, with the two columns showing orthogonal projections. The two projections are edge-on views of the central galaxy, with the satellite plane being shown edge-on and face-on in the left- and right-hand columns, respectively. The blue hue shows the distribution of stars which is dominated by the central galaxy. The luminous satellites are shown as grey circles with sizes varying according to their stellar mass. The dotted line shows the best-fitting plane of the central galaxy while the dashed line in the left-hand column shows the best-fitting plane of the satellite system. The top left-hand text insert gives the shape of the satellite system and its angle with respect to the central galaxy.

We focus our analysis on the misalignment angle between the minor axes because a large fraction of central galaxies are discs and hence have $a \approx b$ which makes it difficult to identify robustly the major and intermediate axes (see Fig. 3). In contrast, $c \leq b$ for all systems, independently of whether we measure the shape of the halo, central galaxy or satellite system. While not discussed, we have also studied the alignment between the major axes of the various components and found it to be weaker than the alignment of the minor axes, while the intermediate axes show a very weak alignment, if any at all.

2.4 Disc and spheroid galaxy samples

We split the centrals into disc and spheroidal galaxies, following the procedure of Scannapieco et al. (2009, see also Sales et al. 2012) and divide our sample according to the degree of ordered rotation. We define the parameter, $\kappa_{\rm rot}$, as the fraction of kinetic energy, K, invested in ordered rotation, i.e.

$$\kappa_{\rm rot} \equiv \frac{K_{\rm rot}}{K} = \frac{\sum_j \frac{1}{2} m_j [(\hat{\boldsymbol{L}} \times \hat{\boldsymbol{r}}_j) \cdot \boldsymbol{v}_j]^2}{\sum_j \frac{1}{2} m_j \boldsymbol{v}_j^2}, \quad (3)$$

where $\boldsymbol{v}_j$, $\hat{\boldsymbol{r}}_j$ and m_j are the velocity, unit position vector and mass of the jth star particle in the centre of mass reference frame and $\hat{\boldsymbol{L}}$ is the direction of the total angular momentum of the stellar component of central galaxy. For perfect circular motion $\kappa_{\rm rot} = 1$, while for non-rotating systems, $\kappa_{\rm rot} \ll 1$. In practice, we classify the galaxies with $\kappa_{\rm rot} \geq 0.6$ and $\kappa_{\rm rot} \leq 0.45$ as discs and spheroids, respectively. This classification results in roughly a third disc galaxies, another third spheroids and the remaining third an intermediate population.

Note that our disc versus spheroid kinematic decomposition differs from the customary photometry-based method used in observational studies, with the two showing a moderate correlation with considerable scatter (Abadi et al. 2003; Scannapieco et al. 2010). Applying the latter method to simulations requires the creation of realistic galaxy images which introduces an additional layer of complexity. We therefore restrict our analysis to galaxies with high and low values of $\kappa_{\rm rot}$, which correspond to the most disc- and spheroid-like objects.

3 RESULTS

In this section we determine the alignment between the three galactic subsystems: the central galaxy, the DM halo and the satellite system. Our analysis is based on haloes with masses similar to that of the MW halo for which EAGLE has just the right volume to include a large number of such objects while having enough resolution to detect their bright satellite populations. We will also characterize the alignment of these galactic subsystems with the surrounding large-scale structure (LSS), which indicates the preferential direction of accretion.

3.1 The shapes of the galactic subsystems

The shapes of the halo, central galaxy and, to a lesser extent, the satellite distribution have been studied extensively in both collisionless and hydrodynamic simulations (e.g. Bett et al. 2010; Wang et al. 2013; Tenneti et al. 2014; Velliscig et al. 2015a). We therefore present only a brief overview of the degree of flattening of these subsystems. Fig. 2 shows the axes or shape ratios, b/a and c/a, for the central galaxy, DM halo and satellite system. The panels show a two-dimensional histogram where each bin is coloured according to the number of systems in that bin as indicated by each colour bar. To the right of each plot, we also show the probability distribution function (PDF) of c/a.

Most central galaxies have a strongly oblate shape ($a \approx b > c \approx 0.5a$), with more than half of the population having $b/a \geq 0.9$ and $0.4 \leq c/a \leq 0.6$ (see top left-hand panel in Fig. 2). The remaining galaxies are also preferentially oblate, though to a lesser extent. Note that due to the use of a Jeans mass limiting pressure floor in the EAGLE prescription for star formation, it is difficult for gas to cool into thin discs before forming stars (for details see Schaye et al. 2015), which results in an artificial thickening of the stellar component and which may explain why there are no galaxies with $c/a \leq 0.3$. The use of a mass- rather than light-weighted inertia tensor also leads to thicker disc.

The DM halo is the closest to spherical of the galactic subsystems shown in Fig. 2, with most haloes having a slightly prolate ($a > b \approx c$) or nearly spherical ($a \approx b \approx c$) shape, in agreement with previous studies (e.g. Frenk et al. 1988; Tenneti et al. 2014).

The satellite systems, both for the full and the 11 most massive objects, have the largest spread in shape parameters, centred on $b/a \approx 0.7$ and $c/a \approx 0.5$. The total population of subhaloes is expected approximately to trace the DM halo shape, so the large spread and the low sphericity (c/a) values of the satellite population reflect systematic effects due to the low number of such objects (Hoffmann et al. 2014) and the biased spatial distribution of the brightest satellites. This can be appreciated in the lower two panels of Fig. 2, with the system of the 11 most massive satellites having systematically lower b/a and c/a values than the full sample of luminous satellites, as noted by Wang et al. (2013). The red symbol in the bottom right-hand panel of Fig. 2 marks the shape of the 11 classical satellites of the MW, $b/a = 0.56 \pm 0.02$ and $c/a = 0.183 \pm 0.008$ (obtained using the positional data from Cautun et al. 2015b). While the b/a value for the MW satellites is typical of the simulated systems, the c/a value is low, with only ≈1 per cent of EAGLE systems having an equal or lower sphericity. This is in agreement with previous studies (e.g. Libeskind et al. 2005; Wang et al. 2013) that have investigated the high flattening of the classical MW satellite plane.

3.2 The alignment of galactic subsystems

We start by studying the alignment between the central galaxy and its host halo, which we show in the top panel of Fig. 3. Since the shape and the main axes of the halo vary as a function of distance from the centre (see e.g. Bett et al. 2010; Velliscig et al. 2015a), we measure the alignment for several radial extents of 10, 50, 100 kpc and R_{200} by plotting the cumulative distribution function (CDF) of $\cos\theta_{\rm C-H}$. The alignment is the strongest between the innermost halo and the central galaxy, most likely due to the dominance of baryons in this inner region, and decreases rapidly as we consider the more extended halo. The entire halo enclosed within R_{200} still shows a substantial alignment with the central galaxy, with half of the sample having a misalignment angle, $\theta_{\rm C-H} \leq 33^\circ$, as shown in Table 1.

Motivated by previous studies which have reported a stronger alignment for spheroidal galaxies (e.g. Tenneti, Mandelbaum & Di Matteo 2015), we show in the bottom panel of Fig. 3 the misalignment angle, $\theta_{\rm C-H}$, separately for disc and spheroid central galaxies. Because of the limited size of the samples (≈350 objects each), we assess the significance of any trend with galaxy morphology using the Kolmogorov–Smirnov (KS) test. The inner 10 kpc halo is more aligned for disc galaxies than for the spheroid population with a KS test significance of 8.3σ. This trend reverses as the radial distance

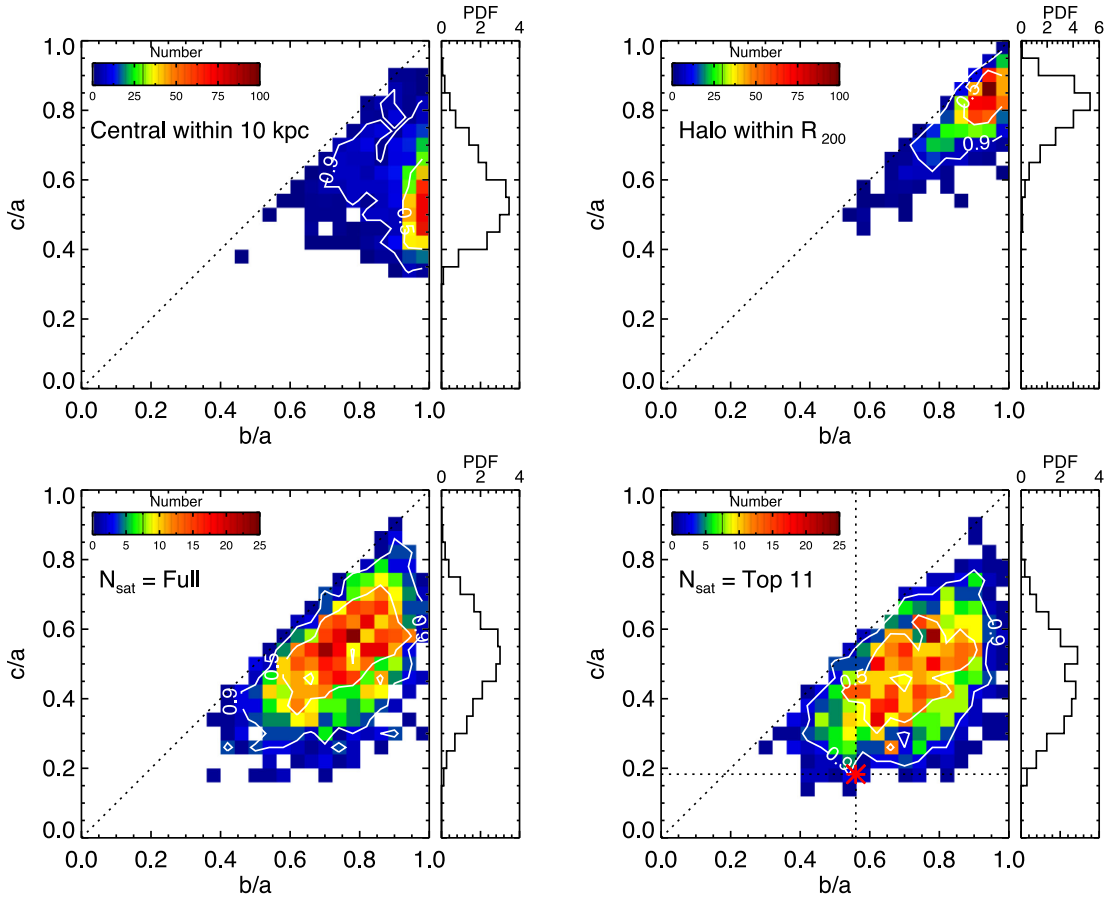

Figure 2. The distribution of the shape parameters, b/a and c/a, for central galaxies (top-left), DM haloes (top-right), all the luminous satellites (bottom-left) and the 11 most massive satellites, ranked by stellar mass (bottom-right). The shapes are computed using all the star particles within 10 kpc for the central galaxy, all the DM particles within R_{200} for the halo, and the luminous satellites within a distance of 300 kpc from the central galaxy. The colours indicate the number of systems in each bin with the corresponding numbers given in the top left-hand colour bar. The two solid contours indicate the regions enclosing 50 and 90 per cent of the sample. The right-hand side of each plot shows the PDF of c/a. The red symbol in the bottom right-hand panel shows the axis ratios for the MW's 11 classical satellites.

used to compute the halo shape increases such that the entire, R_{200}, halo is more aligned with spheroids than with discs, at a KS significance of 3.7σ. These results are consistent with observational data (e.g. Yang et al. 2006, for more details see the discussion section) and with other hydrodynamical simulations (e.g. Tenneti et al. 2015), but are contrary to the results of Velliscig et al. (2015a), which found that disc galaxies are better aligned with their haloes than spheroidal ones. The discrepancy is due to the method used to classify the galaxies into discs and spheroids. Velliscig et al. (2015a) used the ratio of the SUBFIND velocity dispersion to the maximum circular velocity, while we used the fraction of the kinetic energy in ordered rotation that, with hindsight, is a better kinematical indicator of galaxy morphology.

In Fig. 4, we compare the alignment between the satellite system and its host halo, again with the halo shape measured as function of distance from the centre. In contrast to the central–halo alignment, the satellites are more aligned with the entire halo and to a much lesser extent with the inner regions of the halo. This is to be expected, since the satellite system is more extended than the central galaxy and is thus more likely to trace the outer halo.

Fig. 5 shows that there is an alignment, albeit weak, between the central galaxies and their satellite systems. The alignment strength is very similar if we consider the full set of luminous satellites in EAGLE (solid line) or only the 11 most massive satellites (dashed line), which would correspond to the classical satellites of the MW. The bottom panel of Fig. 5 shows that spheroid centrals are more aligned with their satellite systems than disc centrals, though in both cases the alignment is weak. The dependence of alignment on central morphology is robust, having a KS test significance of 3.0σ.

The alignment between central galaxies and their satellites, as measured in EAGLE, is important to better understand the two major satellite systems in the LG. For this, we computed the misalignment angle, $\theta_{\rm C-S}$, of the MW and M31 systems, whose values are shown by two vertical arrows in the top panel of Fig. 5. In the case of the MW, we considered only the 11 classical satellites, since observations of fainter satellites are more strongly affected by incomplete survey area and incompleteness. Using the coordinates and uncertainties from McConnachie (2012), we computed a misalignment angle, $\theta_{\rm C-S;\,MW} = 78^\circ$, $\cos\theta_{\rm C-S;\,MW} = 0.21 \pm 0.01$, between the disc of the MW and its 11 classical satellites. In the case of M31, using the McConnachie (2012) catalogue, we selected as satellite galaxies brighter than -8.8 in absolute V-band magnitude (equal to the faintest classical MW satellite) that is within a 3D distance of 300 kpc from M31. This resulted in 18 satellites whose spatial distribution has axis ratios, $b/a = 0.72^{+0.07}_{-0.06}$ and $c/a = 0.61^{+0.03}_{-0.04}$, and has a misalignment angle, $\theta_{\rm C-S;\,M31} = 80^{\circ\,+6}_{-5}$, i.e. $\cos\theta_{\rm C-S;\,M31} = 0.17^{+0.09}_{-0.10}$, with the disc of M31. We quote 1σ uncertainties due to errors in the distance of the M31 satellites.

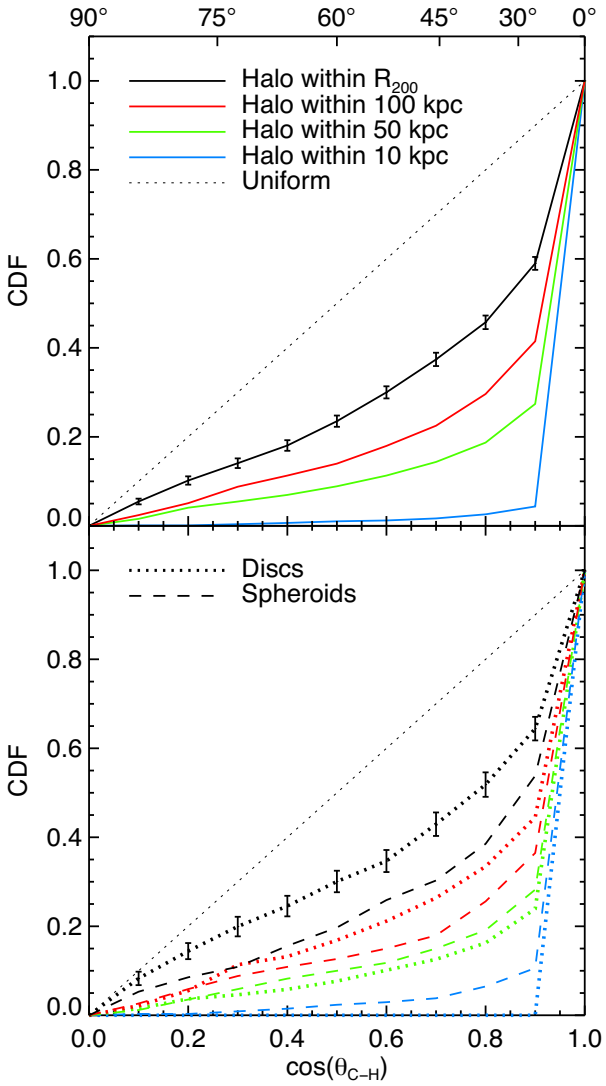

Figure 3. Top panel: the CDF of the misalignment angle, $\cos\theta_{\rm C-H}$, between the minor axes of the central galaxy and the host DM halo. The various lines show the dependence of the alignment strength on the region used to determine the halo shape, which we measure within spherical regions of radii 10, 50, 100 kpc and R_{200}. Bottom panel: same as the top panel, but with the central galaxies divided into discs (dotted line) and spheroids (dashed line). The error bars show the 1σ bootstrap uncertainty. The thin dotted line in both panels corresponds to the CDF of a uniform distribution.

Table 1. The misalignment angle, θ (columns 5–7), and its cosine, $\cos\theta$ (columns 2–4), corresponding to 25, 50 and 75 per cent of the population. Bootstrap resampling gives an uncertainty of ±0.015 in the value of $\cos\theta$. The corresponding uncertainty for θ depends on the value of the angle and ranges from $\pm3^\circ$ for small angles to $\pm1^\circ$ for large angles.

Alignment type	$\cos\theta$			θ (°)		
	25 per cent	50 per cent	75 per cent	25 per cent	50 per cent	75 per cent
Central–halo	0.52	0.84	0.96	58	33	17
Satellites–halo	0.58	0.83	0.95	55	34	19
Halo–LSS	0.48	0.78	0.93	61	39	22
Satellites–LSS	0.38	0.66	0.85	68	49	32
Central–LSS	0.33	0.63	0.85	71	51	32
Central–satellites	0.30	0.61	0.84	73	52	33
Uniform	0.25	0.50	0.75	76	60	41

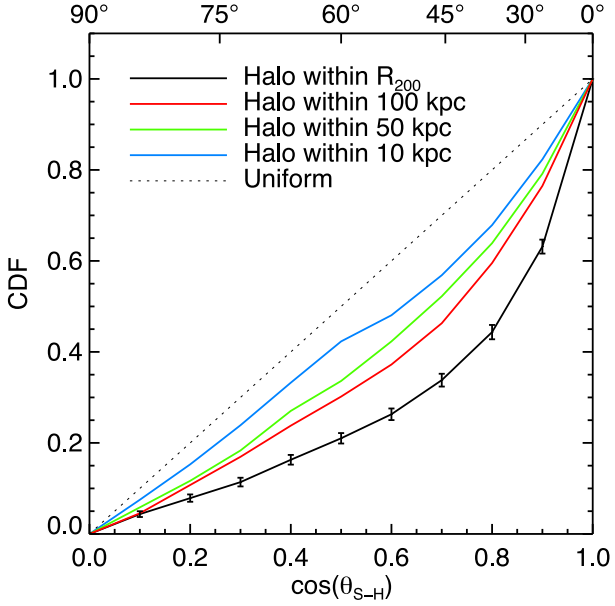

Figure 4. The CDF of the misalignment angle, $\cos\theta_{\rm S-H}$, between the minor axes of the satellite system and the host DM halo, with the halo shape measured within various radial distances.

Thus, both the MW and M31 have systems of bright satellites that are nearly perpendicular to their disc. Such configurations are quite common, with ≈20 per cent of the EAGLE systems having misalignment angles at least as extreme as the MW and M31. A notable feature of the classical MW satellites is that they are distributed along a thin plane, so we checked if the central–satellite system alignment is correlated to the shape of the satellite distribution and find no such dependence. Fig. 1 shows a selection of five such systems, i.e. with $\theta_{\rm C-S} \geq 78^\circ$. Each panel shows two perpendicular views of the distributions of stars and satellites in those haloes. Some of these systems, like those shown in the middle three panels, have thin satellite planes, i.e. $c/a \sim 0.2$, that are also nearly perpendicular on their central galaxy, as is the case for our own Galaxy.

3.3 Conditional alignments: the key to a better understanding

We found that both the central galaxies and the satellite systems have a strong alignment with a third component, the DM halo. This naturally gives rise to an indirect, or secondary, alignment between the central galaxies and their satellites since both are aligned with their DM haloes. In the following, we wish to investigate if this effect can explain the weak alignment between centrals and their satellite systems. We do so by studying *conditional* alignments, that is, alignments of a subsample of objects that satisfy a certain condition.

If the central–satellite alignment is not just a by-product of the alignment of both components with the halo we would expect a stronger alignment for systems in which the halo and the central are aligned. This arises because the satellites will feel the combined coherent effect of being aligned with both the halo and the central galaxy. This effect is studied in Fig. 6 where we show the satellite–halo alignment *conditional* on the central–halo misalignment angle, $\theta_{\rm C-H}$. We split our sample into three subsamples according to the value of $\theta_{\rm C-H}$ as follows: aligned, $\theta_{\rm C-H} \in [0^\circ, 30^\circ]$; intermediate, $\theta_{\rm C-H} \in [30^\circ, 60^\circ]$; and perpendicular, $\theta_{\rm C-H} \in [60^\circ, 90^\circ]$. As Fig. 6 shows, all three subsamples have the same degree of alignment

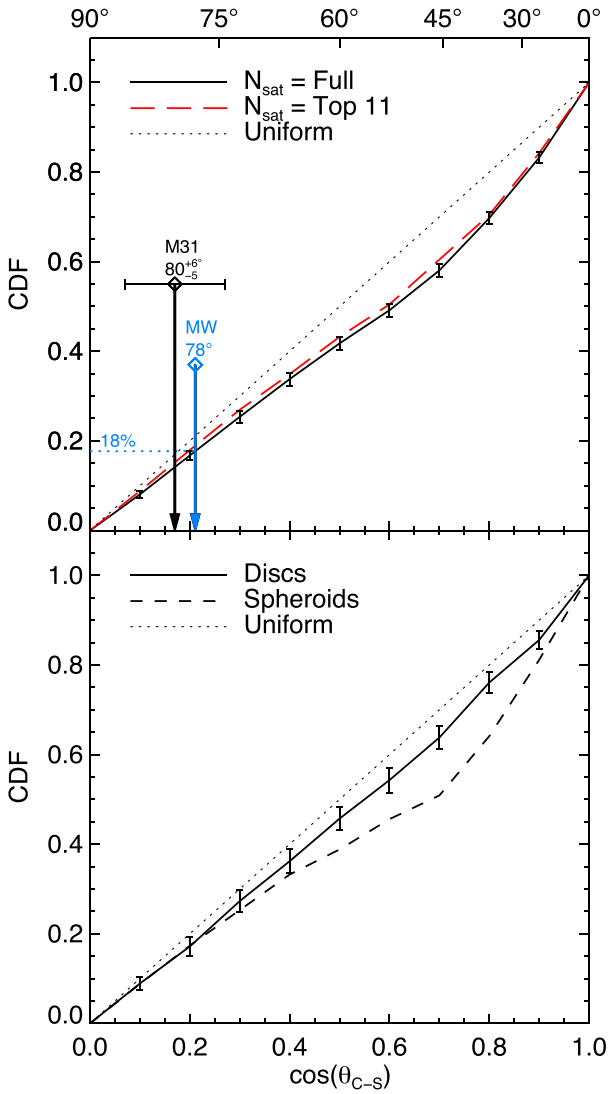

Figure 5. The CDF of the misalignment angle, $\cos\theta_{C-S}$, between the minor axes of the central galaxy and the satellite system. Top panel: the solid line indicates the alignment of the full set of satellites while the dashed line shows the alignment of the most massive 11 satellites. The right-hand vertical arrow shows the misalignment angle, $\theta_{C-S;\,MW} = 78^\circ$, for the MW system while the left-hand vertical arrow with error bars shows the misalignment angle, $\theta_{C-S;\,M31} = 80^{\circ}{}^{+6}_{-5}$, and its 1σ range for the M31 system. Bottom panel: the alignment of the full set of satellites with disc (solid) and spheroid (dashed) central galaxies.

between the satellites and the halo as the overall sample, suggesting that the central galaxy does not directly influence the orientation of the satellite system.

Fig. 7 shows a complementary test where, using the same subsamples as in Fig. 6, we show the *conditional* alignment between centrals and their satellites. The misalignment degree varies vastly between subsamples: the centrals that are more aligned with their haloes are also the ones that are more aligned with their satellite systems.

To summarize, the central–satellite alignment is a consequence of the tendency of both components to align with the halo. This result has important applications since it can be used to predict with some confidence the orientation of the DM halo from the orientation of its galaxies only, as illustrated in Fig. 8. The figure shows that if

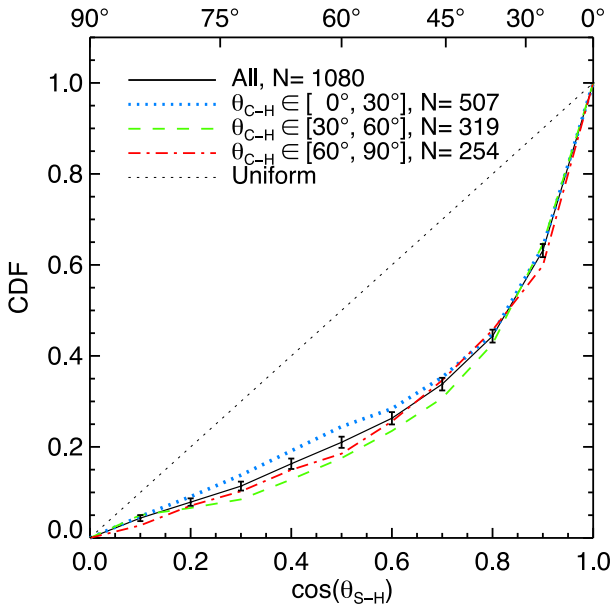

Figure 6. The *conditional* alignment, $\cos\theta_{S-H}$, between satellite systems and their DM haloes given the misalignment angle, θ_{C-H}, between the centrals and their DM haloes. We show the alignment of the full sample (solid line) and that of various subsamples selected according to the value of θ_{C-H}. The subsamples correspond to the central and halo being: aligned, $0^\circ \leq \theta_{C-H} \leq 30^\circ$ (dotted line); intermediate, $30^\circ < \theta_{C-H} \leq 60^\circ$ (dashed line); and perpendicular, $60^\circ < \theta_{C-H} \leq 90^\circ$ (dashed–dotted line). See the plot legend for the number of systems in each subsample.

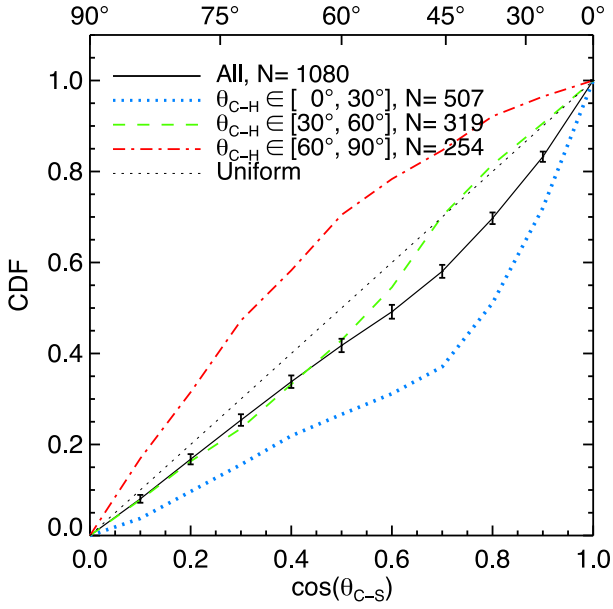

Figure 7. Same as Fig. 6, but for the *conditional* alignment, $\cos\theta_{C-S}$, between centrals and their satellite systems given the misalignment angle, θ_{C-H}, between the centrals and their DM haloes.

the central and the satellite system are aligned ($\theta_{C-S} \leq 30^\circ$), then the DM halo system also tends to point to the same direction. In contrast, if the satellite system is perpendicular to the disc of the central ($\theta_{C-S} \geq 60^\circ$), as in the case of the MW and M31, then the DM halo is only poorly aligned with the central. The dependence on θ_{C-S} is strong, with the median central–halo misalignment angle,

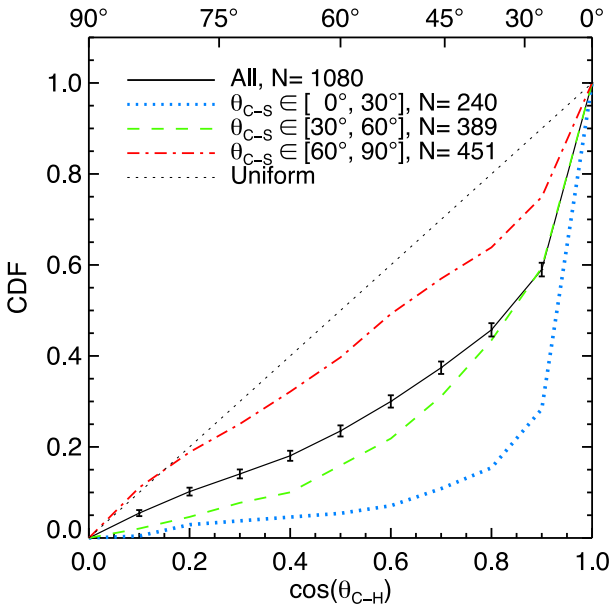

Figure 8. Same as in Fig. 6, but for the *conditional* alignment, $\cos\theta_{\rm C-H}$, between centrals and their DM haloes given the misalignment angle, $\theta_{\rm C-S}$, between the centrals and their satellite systems.

which is 33° for the entire sample, varying from 18° for $\theta_{\rm C-S} \leq 30°$ to 52° for $\theta_{\rm C-S} \geq 60°$.

3.4 The alignment with the large-scale structure

Within the standard model, DM, gas and satellites are accreted predominantly along filaments, which determine a common preferred axis (e.g. Libeskind et al. 2005, 2011, 2014; Deason et al. 2011; Lovell et al. 2011). Thus, we would expect the halo, central and satellite system to be aligned with the LSS in which they are embedded (e.g. Tempel et al. 2015; Velliscig et al. 2015b; Welker et al. 2015).

We measure the orientation of the LSS by computing the moment of inertia of the matter within the spherical shell located between $2R_{200}$ and $3R_{200}$ from the centre of each halo. We then compute the misalignment angle between the minor axes of the galactic subsystems and that of the LSS. The resulting alignment is shown in Fig. 9. We find that all three galactic components show some degree of alignment with their surrounding distribution of matter: the halo–LSS alignment is the largest, followed by the satellite–LSS and central–LSS alignments (see Table 1 for a comparison to the alignment between galactic components). We note that the alignment with the LSS decreases rapidly if we were to measure the LSS directions using spherical shells of larger radii.

In Section 3.3, we found that the central–satellites alignment is a consequence of both components being aligned with a third, the DM halo. Since the LSS shows a considerable alignment with the halo, we studied if the satellite–LSS and central–LSS alignments are a consequence of the same effect. The former is investigated in Fig. 10, where we show the satellite–halo alignment for subsamples selected according to the halo–LSS misalignment angle, $\theta_{\rm H-LSS}$. We find that the satellite–halo alignment is weaker for higher values of $\theta_{\rm H-LSS}$, i.e. when the halo is close to perpendicular to the LSS. Thus, the satellite system is more strongly aligned with the LSS than would be expected from the fact that both are aligned with the halo. In contrast, the central–LSS alignment is a consequence of the tendency of both components to be aligned with the halo. Applying

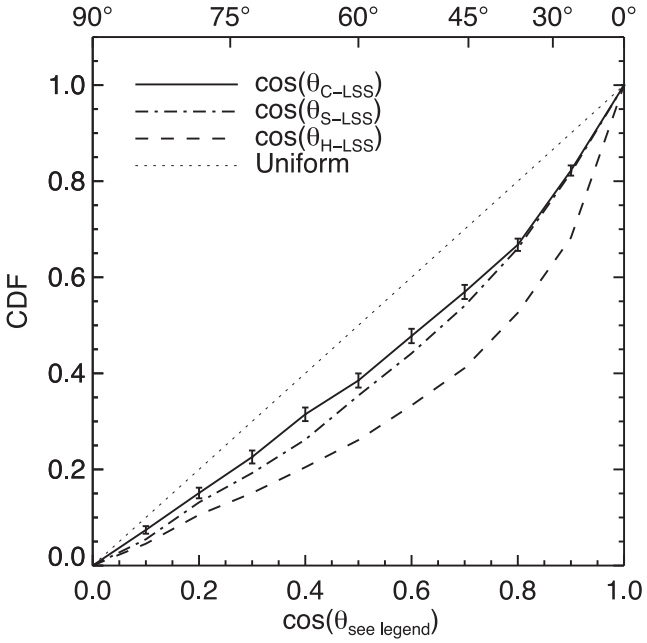

Figure 9. The CDF of the misalignment angles of the various galactic subsystems with the LSS in which they are embedded (on scales of 2–$3R_{200}$). The solid line shows the central galaxy–LSS alignment, $\cos\theta_{\rm C-LSS}$; the dashed–dotted line the satellite system–LSS alignment, $\cos\theta_{\rm S-LSS}$; and the dashed line the halo–LSS alignment, $\cos\theta_{\rm H-LSS}$.

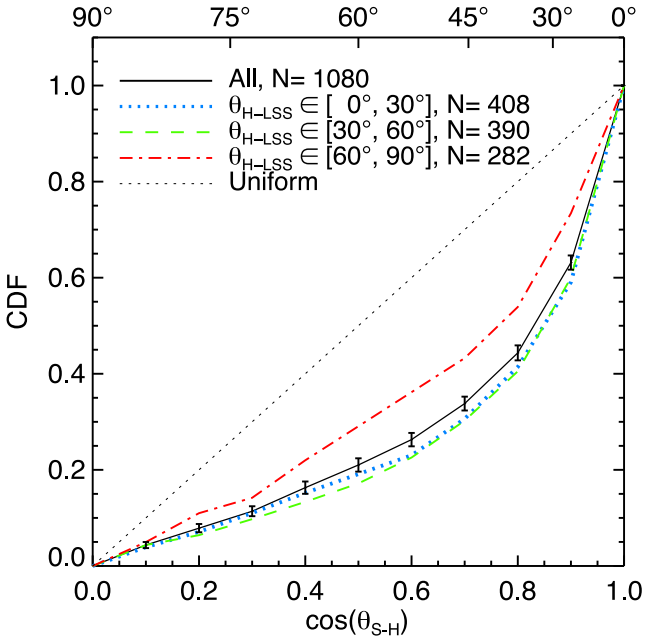

Figure 10. Same as Fig. 6, but for the *conditional* alignment, $\cos\theta_{\rm S-H}$, between satellite systems and their DM halo given the misalignment angle, $\theta_{\rm H-LSS}$, between the DM haloes and the LSS within which they are embedded (on scales of 2–$3R_{200}$).

the same test as in Fig. 10 to the central–halo alignment, we found no significant trend with $\theta_{\rm H-LSS}$.

4 DISCUSSION

We have studied the alignment between the central galaxy, satellite system and DM halo as well as that of the LSS within which they

are embedded. The sample consists of 1080 MW-mass systems (of typical mass $\sim 10^{12}\,M_{\odot}$) that have at least 11 luminous satellites within 300 kpc, similar to the MW and M31 systems. This sample was selected from the largest of the EAGLE hydrodynamical simulation, which is an ideal tool for our study. First, the EAGLE simulation has been calibrated to reproduce the observed galaxy stellar mass function and the observed size–mass relation (Crain et al. 2015; Schaye et al. 2015). Secondly, the resolution of EAGLE is sufficient to identify luminous satellites that are comparable to the classical dwarf satellites of the MW while providing a large enough sample of MW-mass haloes. In the following, we discuss the major results of this work.

4.1 Alignments with the DM halo

We find that central galaxies tend to be well aligned with their DM host haloes, with a median misalignment angle of 33°, which is in good agreement with previous studies (e.g. Bett et al. 2010; Tenneti et al. 2014; Velliscig et al. 2015a). The centrals show an even larger degree of alignment with the inner halo (Bett et al. 2010; Deason et al. 2011; Velliscig et al. 2015a), with most centrals being nearly parallel to the halo orientation within 50 kpc or less. Bailin et al. (2005) found the same result and argued that in the inner ∼20 kpc region the baryonic and DM components exert a similar torque on each other and thus are equally responsible for their very strong alignment.

While the centrals tend to be very well aligned with the inner 10 kpc halo, Fig. 3 also shows that this inner 10 kpc halo is only partially aligned with the outer halo, with a median misalignment angle of 33°. This misalignment is stronger than that measured in DM-only simulations, with Bailin & Steinmetz (2005) reporting a median misalignment angle of ≈25°. The increased misalignment is likely due to the presence of baryons that affect the orientation of the inner halo while hardly affecting the outer halo (Bailin et al. 2005).

The satellite system is misaligned with the entire halo to the same extent as the central galaxy is, as can be seen from Fig. 11. This is somewhat surprising, since many satellites are found in the outer regions of the halo, and may thus be expected to trace the entire halo quite well. Note that we do find that the satellites are more misaligned with the inner halo than with the entire halo and thus they do preferentially trace the outer halo. This misalignment between satellites and their host halo can be attributed to two causes. First, the misalignment is partially due to the relatively small number of satellites per halo (on average 15), which means that Poisson noise plays an important role (Hoffmann et al. 2014). Secondly, the accretion of the most massive satellites is more anisotropic than that of the components that provide the bulk of the mass of the halo, which are lower mass subhaloes and smooth accretion (Libeskind et al. 2014). This can lead to intrinsic differences between the luminous satellites and the DM halo.

Individually, neither the central galaxy nor the satellite population are very good predictors of the orientation of the DM halo. But, by combining the two components, we can find a subsample that shows a much smaller misalignment angle with the halo. This subsample consists of systems in which the central is nearly parallel to the satellite system, for which the median central–halo misalignment angle is just 18°. Using a sample with these characteristics would greatly improve the ability to measure the mean flattening of the DM halo using stacked lensing maps (see Bett 2012, and references therein), which currently is limited due to the broad distribution of central–halo misalignment angles. Since 3D satellite positions are currently restricted to the nearby Universe, more work is needed to understand if a similar relation would hold when using projected satellite distributions. Similarly to the central–satellite alignment, the central–LSS alignment is also a consequence of the tendency of both components to align with the halo. So, potentially, to obtain a stronger central–halo alignment, one could also select systems in which the central is nearly parallel to the LSS.

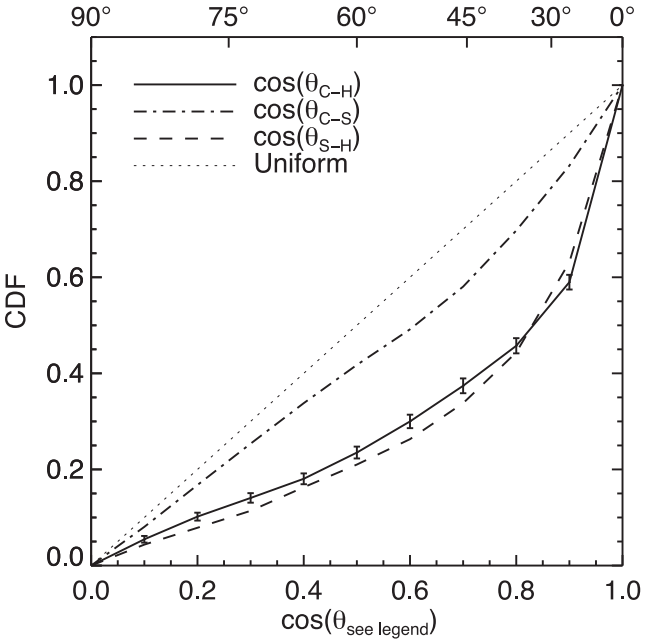

Figure 11. A summary of the alignment between the central galaxies (C), their satellite systems (S) and their entire DM haloes (H), i.e. within R_{200}. The plot shows the CDF of the misalignment angle, θ, between: centrals and their haloes (solid line), satellite systems and their haloes (dashed line) and centrals and their satellites (dash–dotted line).

4.2 The central–satellite system alignment

We also studied the alignment between the central galaxy and the orientation of the entire system of satellites. This is different from most other studies, which measured the alignment between the position of individual satellites and the preferential axes of their central. We found a weak central–satellite system alignment that suggests that satellites are somewhat more likely to be found along the plane of the central galaxy (see also Velliscig et al. 2015b). This is in agreement with Yang et al. (2006, see also Sales & Lambas 2004; Brainerd 2005; Wang et al. 2008, 2010) who measured the same tendency in observational data. More interestingly, we found that the central–satellite system alignment is a by-product of the tendency of both components to align with the halo (see also Agustsson & Brainerd 2010; Wang et al. 2013).

4.3 Dependence on galaxy type

We classified our sample into disc (rotating) and spheroid (non-rotating) subsamples based on the fraction of the kinematic energy in ordered rotation of each central galaxy, as described in Section 2.4. We found that spheroidal galaxies tend to be more aligned with both their haloes and their satellite systems. This difference in alignment strength between spheroids and discs is statistically significant at the more than 3σ level. Surprisingly, the inner halo shows the opposite

trend, being more strongly aligned with discs than with spheroids, with an 8σ significance.

Compared to observations, if we refer to discs as blue (late type) galaxies and to spheroids as red (early type) galaxies, our result is in agreement with the findings of Yang et al. (2006): red centrals show a strong alignment with their satellites, while blue centrals have roughly isotropically distributed satellites. The cause of the trend in alignment strength with the morphology of the central is a topic of debate (e.g. see Yang et al. 2006; Kang et al. 2007). At least for our sample, we checked that this trend is not due to spheroidal centrals being located in more massive haloes than disc centrals. The trend in alignment strength could be related to the properties of the central galaxies themselves, e.g. discs, due to their higher specific angular momentum, are harder to torque than spheroids.

4.4 The connection to the large-scale distribution of matter

We found that the halo, central and satellite system tend to align with the LSS in which they are embedded (on scales of 2–3R_{200}), with the former showing the strongest alignment. This agrees with observational studies that also found that both central and satellite galaxies are aligned with the preferential directions of the cosmic web (Paz et al. 2011; Zhang et al. 2013; Libeskind et al. 2015; Tempel et al. 2015). We also found that the central–LSS alignment is a consequence of both aligning with the DM halo. In turn, this results in spheroid galaxies being slightly better aligned with the LSS than discs since spheroids are more aligned with their host haloes. This trend with central morphology is seen in observations too, with Zhang et al. (2013) finding that red centrals are more strongly aligned with the cosmic web than blue centrals.

The absolute strength of the alignment with the LSS depends on the scale used to determine the LSS orientation, with a larger scale resulting in a smaller alignment. In this paper, we used the mass distribution between two and three times the virial radius, R_{200}, of each halo, which corresponds to scales of 0.5–1 Mpc to define the LSS. These scales are considerably smaller than those available to observations, which are typically a few Mpc. Thus, while we find the same qualitative results as previous studies, from a quantitative perspective we have stronger alignments between the galactic subsystems and the LSS.

4.5 Implications for the MW and M31

The EAGLE simulation indicates that configurations similar to the MW and M31, in which the satellite population is nearly perpendicular to the central disc, are quite common. This result was hinted by the hydrodynamical simulations of Libeskind et al. (2007) who found one such perpendicular configuration in their sample of just three galaxies. In fact, ≈20 per cent of systems have a misalignment angle larger than the MW or M31, which have $\theta_{\rm C-S;\,MW} = 78^\circ$ and $\theta_{\rm C-S;\,M31} = 80^{\circ\,+6}_{\,-5}$, respectively. This large fraction of perpendicular systems is due to the weak alignment between centrals and their satellite systems, which is close to a uniform distribution.

We also predict that the minor axes of the inner ∼10 kpc haloes should be parallel to the normal of the disc planes of the MW and M31, since the alignment for disc galaxies is very strong. In contrast, the outer halo should be only weakly aligned with the central galaxy since, as may be seen in Fig. 8, the satellite systems of the MW and M31 are nearly perpendicular to their central galaxies. We therefore expect the orientation and shape of the halo in these galaxies to vary significantly with radius, a feature that should be taken into account when modelling, for example, the dynamics of MW streams and halo stars (for details see Vera-Ciro & Helmi 2013).

Recently, Libeskind et al. (2015) analysed the alignment with the LSS of several nearby satellite planes: the one in the MW, the two in M31 (Ibata et al. 2013; Shaya & Tully 2013) and the two in the Centaurus A Group (Tully et al. 2015). They found that four out of the five planes, i.e. all except the one in the MW, are nearly parallel (largest misalignment angle is ≈14°) to the minor axis of the cosmic web. Such a result is surprising, since we found a median satellite system–LSS misalignment angle of 49°, which is likely to be much higher when determining the LSS orientation on a 2.5 Mpc scale, as done by Libeskind et al. (see the discussion in Section 4.4). The strong alignment of these satellite planes with the LSS could be due to the particular environment of the LG and its immediate neighbourhood which may not be representative of the Universe as a whole. Alternatively, it may not be appropriate to compare our results with those of Libeskind et al. (2015), since their planes consist of subpopulations of satellites that form spatially thin configurations (for details see Cautun et al. 2015b) and not of the entire satellite populations, as we have considered in this study. Further work is needed to clarify the puzzling alignments detected by Libeskind et al. (2015) between satellite planes and the cosmic web.

5 CONCLUSIONS

We have studied the alignments of the central galaxy, DM halo and satellite system at the present-day in the EAGLE hydrocosmological simulation. EAGLE self-consistently incorporates the main physical processes that affect galaxy and halo shapes as well as the orbits of satellite galaxies, and is therefore ideal for our study. Our sample consists of MW-mass haloes (of typical mass $\sim 10^{12}\,{\rm M}_\odot$) that have at least 11 luminous satellites within a radius of 300 kpc; we found 1080 such systems in EAGLE. The main axes were determined from the moment of inertia measured within 10 kpc for centrals, R_{200} for haloes and 300 kpc for the satellite system. We focused on the misalignment angle between the minor axes of the galactic components since the major and intermediate axes show a lesser degree of alignment.

Our main conclusions are as follows.

(i) The central galaxies and the satellite systems tend to be well aligned with their host haloes, with a median misalignment angle of ≈33° in both cases (see Table 1). On the other hand, the centrals and their satellites are only weakly aligned with one another (see Fig. 11).

(ii) The alignment strength depends on the radial extent of the DM halo considered. The alignment of central galaxies is largest with the inner 10 kpc of the halo and decreases with increasing radial extent (see Fig. 3). In contrast, the satellite system is better aligned with the entire halo, as measured within R_{200}, and less well aligned with the inner halo (see Fig. 4).

(iii) Spheroidal centrals are better aligned with both their halo and their satellite system than disc centrals (see Figs 3 and 5).

(iv) The weak alignment between centrals and their satellites is a consequence of the tendency of both components to be aligned with the DM halo (see Figs 6 and 7).

(v) The orientation of the halo can be tightly constrained in systems where the centrals and satellite systems are close to parallel, with such subsamples having a median central–halo misalignment angle of only 18°. In contrast, systems where the central and satellite systems are nearly perpendicular, as is the case for the MW and M31, show a much weaker central–halo alignment (see Fig. 8).

(vi) The central, halo and satellites tend to be aligned, to various degrees, with the large-scale distribution of matter in which they

are embedded (see Fig. 9). While the central–LSS alignment is a consequence of both components being somewhat aligned with the halo, the satellite–LSS alignment is stronger than expected from such an effect alone (see Fig. 10).

To conclude, our goal was to better understand the seemingly puzzling situation around the MW and M31 where the configurations of bright satellites are nearly perpendicular to the disc of their centrals. Because of the weak alignment between centrals and their satellites, such perpendicular configurations are in fact quite common, with ≈20 per cent of EAGLE systems having misalignment angles at least as extreme as the MW and M31. The perpendicular configuration also implies that the directions of the MW and M31 haloes cannot be constrained from the orientation of their centrals, since such systems have only a very weak central–halo alignment.

ACKNOWLEDGEMENTS

We thank Aaron Ludlow, Wenting Wang and Jie Wang for helpful discussions and suggestions. We also thank the anonymous referee for comments that have helped us improve the paper. MC, CSF and MS were supported in part by ERC Advanced Investigator grant COSMIWAY (grant number GA 267291), the Science and Technology Facilities Council (grant number ST/F001166/1, ST/I00162X/1). LG acknowledges support from the NSFC grant (Nos 11133003, 11425312), the Strategic Priority Research Program 'The Emergence of Cosmological Structure' of the Chinese Academy of Sciences (No. XDB09000000), and a Newton Advanced Fellowship, as well as the hospitality of the Institute for Computational Cosmology at Durham University. RAC is a Royal Society University Research Fellow. JS acknowledges the ERC Grant agreement 278594-GasAroundGalaxies. TT acknowledges the Interuniversity Attraction Poles Programme initiated by the Belgian Science Policy Office ([AP P7/08 CHARM]). This work used the DiRAC Data Centric system at Durham University, operated by ICC on behalf of the STFC DiRAC HPC Facility (www.dirac.ac.uk). This equipment was funded by BIS National E-infrastructure capital grant ST/K00042X/1, STFC capital grant ST/H008519/1, and STFC DiRAC Operations grant ST/K003267/1 and Durham University. DiRAC is part of the National E-Infrastructure. We acknowledge PRACE for awarding us access to the Curie machine based in France at TGCC, CEA, Bruyères-le-Châtel.

REFERENCES

Abadi M. G., Navarro J. F., Steinmetz M., Eke V. R., 2003, ApJ, 591, 499
Agustsson I., Brainerd T. G., 2010, ApJ, 709, 1321
Aubert D., Pichon C., Colombi S., 2004, MNRAS, 352, 376
Bailin J., Steinmetz M., 2005, ApJ, 627, 647
Bailin J. et al., 2005, ApJ, 627, L17
Bett P., 2012, MNRAS, 420, 3303
Bett P., Eke V., Frenk C. S., Jenkins A., Helly J., Navarro J., 2007, MNRAS, 376, 215
Bett P., Eke V., Frenk C. S., Jenkins A., Okamoto T., 2010, MNRAS, 404, 1137
Booth C. M., Schaye J., 2009, MNRAS, 398, 53
Brainerd T. G., 2005, ApJ, 628, L101
Buck T., Macciò A. V., Dutton A. A., 2015, ApJ, 809, 49
Buck T., Dutton A. A., Macciò A. V., 2016, preprint (arXiv:1510.06028)
Cautun M., Frenk C. S., van de Weygaert R., Hellwing W. A., Jones B. J. T., 2014, MNRAS, 445, 2049
Cautun M., Wang W., Frenk C. S., Sawala T., 2015a, MNRAS, 449, 2576
Cautun M., Bose S., Frenk C. S., Guo Q., Han J., Hellwing W. A., Sawala T., Wang W., 2015b, MNRAS, 452, 3838
Chabrier G., 2003, PASP, 115, 763
Conn A. R. et al., 2013, ApJ, 766, 120
Crain R. A. et al., 2015, MNRAS, 450, 1937
Dalla Vecchia C., Schaye J., 2012, MNRAS, 426, 140
Davis M., Efstathiou G., Frenk C. S., White S. D. M., 1985, ApJ, 292, 371
Deason A. J. et al., 2011, MNRAS, 415, 2607
Dolag K., Borgani S., Murante G., Springel V., 2009, MNRAS, 399, 497
Dong X. C., Lin W. P., Kang X., Ocean Wang Y., Dutton A. A., Macciò A. V., 2014, ApJ, 791, L33
Fardal M. A. et al., 2013, MNRAS, 434, 2779
Frenk C. S., White S. D. M., Davis M., Efstathiou G., 1988, ApJ, 327, 507
Haardt F., Madau P., 2001, in Neumann D. M., Tran J. T. V., eds, Clusters of Galaxies and the High Redshift Universe Observed in X-rays (arXiv:astro-ph/0106018)
Han J., Wang W., Cole S., Frenk C. S., 2016, MNRAS, 456, 1017
Hoffmann K. et al., 2014, MNRAS, 442, 1197
Hopkins P. F., 2013, MNRAS, 428, 2840
Ibata R. A. et al., 2013, Nature, 493, 62
Ibata R. A., Ibata N. G., Lewis G. F., Martin N. F., Conn A., Elahi P., Arias V., Fernando N., 2014, ApJ, 784, L6
Kang X., van den Bosch F. C., Yang X., Mao S., Mo H. J., Li C., Jing Y. P., 2007, MNRAS, 378, 1531
Knebe A., Gill S. P. D., Gibson B. K., Lewis G. F., Ibata R. A., Dopita M. A., 2004, ApJ, 603, 7
Kroupa P., Theis C., Boily C. M., 2005, A&A, 431, 517
Kunkel W. E., Demers S., 1976, in Dickens R. J., Perry J. E., Smith F. G., King I. R., eds, Royal Greenwich Observatory Bulletins, Vol. 182, The Galaxy and the Local Group. Royal Greenwich Observatory, Herstmonceaux, p. 241
Li Y.-S., Helmi A., 2008, MNRAS, 385, 1365
Libeskind N. I., Frenk C. S., Cole S., Helly J. C., Jenkins A., Navarro J. F., Power C., 2005, MNRAS, 363, 146
Libeskind N. I., Cole S., Frenk C. S., Okamoto T., Jenkins A., 2007, MNRAS, 374, 16
Libeskind N. I., Frenk C. S., Cole S., Jenkins A., Helly J. C., 2009, MNRAS, 399, 550
Libeskind N. I., Knebe A., Hoffman Y., Gottlöber S., Yepes G., Steinmetz M., 2011, MNRAS, 411, 1525
Libeskind N. I., Knebe A., Hoffman Y., Gottlöber S., 2014, MNRAS, 443, 1274
Libeskind N. I., Hoffman Y., Tully R. B., Courtois H. M., Pomarède D., Gottlöber S., Steinmetz M., 2015, MNRAS, 452, 1052
Lovell M. R., Eke V. R., Frenk C. S., Jenkins A., 2011, MNRAS, 413, 3013
Lynden-Bell D., 1976, MNRAS, 174, 695
Lynden-Bell D., 1982, Observatory, 102, 202
McConnachie A. W., 2012, AJ, 144, 4
Metz M., Kroupa P., Libeskind N. I., 2008, ApJ, 680, 287
Nierenberg A. M., Auger M. W., Treu T., Marshall P. J., Fassnacht C. D., Busha M. T., 2012, ApJ, 752, 99
Pawlowski M. S., Kroupa P., 2013, MNRAS, 435, 2116
Pawlowski M. S., Kroupa P., Angus G., de Boer K. S., Famaey B., Hensler G., 2012, MNRAS, 424, 80
Pawlowski M. S., Kroupa P., Jerjen H., 2013, MNRAS, 435, 1928
Paz D. J., Sgró M. A., Merchán M., Padilla N., 2011, MNRAS, 414, 2029
Piffl T. et al., 2014, A&A, 562, A91
Planck Collaboration XVI, 2014, A&A, 571, A16
Rosas-Guevara Y. M. et al., 2015, MNRAS, 454, 1038
Sales L., Lambas D. G., 2004, MNRAS, 348, 1236
Sales L. V., Navarro J. F., Theuns T., Schaye J., White S. D. M., Frenk C. S., Crain R. A., Dalla Vecchia C., 2012, MNRAS, 423, 1544
Scannapieco C., White S. D. M., Springel V., Tissera P. B., 2009, MNRAS, 396, 696
Scannapieco C., Gadotti D. A., Jonsson P., White S. D. M., 2010, MNRAS, 407, L41
Schaller M., Dalla Vecchia C., Schaye J., Bower R. G., Theuns T., Crain R. A., Furlong M., McCarthy I. G., 2015, MNRAS, 454, 2277
Schaye J., 2004, ApJ, 609, 667
Schaye J., Dalla Vecchia C., 2008, MNRAS, 383, 1210

Schaye J. et al., 2015, MNRAS, 446, 521
Shaya E. J., Tully R. B., 2013, MNRAS, 436, 2096
Shi J., Wang H., Mo H. J., 2015, ApJ, 807, 37
Smith R., Duc P. A., Bournaud F., Yi S. K., 2016, ApJ, 818, 11
Springel V., 2005, MNRAS, 364, 1105
Springel V., Yoshida N., White S. D. M., 2001, New Astron., 6, 79
Springel V., Di Matteo T., Hernquist L., 2005, MNRAS, 361, 776
Tempel E., Guo Q., Kipper R., Libeskind N. I., 2015, MNRAS, 450, 2727
Tenneti A., Mandelbaum R., Di Matteo T., Feng Y., Khandai N., 2014, MNRAS, 441, 470
Tenneti A., Mandelbaum R., Di Matteo T., 2015, preprint (arXiv:1510.07024)
Tully R. B., Libeskind N. I., Karachentsev I. D., Karachentseva V. E., Rizzi L., Shaya E. J., 2015, ApJ, 802, L25
Velliscig M. et al., 2015a, MNRAS, 453, 721
Velliscig M. et al., 2015b, MNRAS, 454, 3328
Vera-Ciro C., Helmi A., 2013, ApJ, 773, L4
Wang Y., Yang X., Mo H. J., Li C., van den Bosch F. C., Fan Z., Chen X., 2008, MNRAS, 385, 1511
Wang Y., Park C., Hwang H. S., Chen X., 2010, ApJ, 718, 762
Wang J., Frenk C. S., Cooper A. P., 2013, MNRAS, 429, 1502
Wang Y. O., Lin W. P., Kang X., Dutton A., Yu Y., Macciò A. V., 2014, ApJ, 786, 8
Wang W., Han J., Cooper A. P., Cole S., Frenk C., Lowing B., 2015, MNRAS, 453, 377
Welker C., Dubois Y., Pichon C., Devriendt J., Chisari E. N., 2015, MNRAS, submitted (arXiv:1512.00400)
Wiersma R. P. C., Schaye J., Smith B. D., 2009a, MNRAS, 393, 99
Wiersma R. P. C., Schaye J., Theuns T., Dalla Vecchia C., Tornatore L., 2009b, MNRAS, 399, 574
Yang X., van den Bosch F. C., Mo H. J., Mao S., Kang X., Weinmann S. M., Guo Y., Jing Y. P., 2006, MNRAS, 369, 1293
Zentner A. R., Kravtsov A. V., Gnedin O. Y., Klypin A. A., 2005, ApJ, 629, 219
Zhang Y., Yang X., Wang H., Wang L., Mo H. J., van den Bosch F. C., 2013, ApJ, 779, 160

APPENDIX A: SAMPLE CHARACTERISTICS

Here, we characterize our sample of MW-like systems in terms of its distribution of halo masses and its satellite mass function.

Our sample is composed of haloes in the mass range, $M_{200} \in [0.3, 3] \times 10^{12}\,\mathrm{M}_\odot$, that contain at least 11 luminous satellite galaxies within a radius of 300 kpc. Fig. A1 shows the resulting halo mass distribution for the full sample as well as for the subsamples split according to the morphology of the central galaxy. The decrease of the mass distribution below $10^{12}\,\mathrm{M}_\odot$ is due to many low-mass haloes not having the required 11 luminous satellites. The weak decrease at higher masses is due to the decreasing halo mass function. We also note that while the spheroidal galaxies have slightly higher halo masses than the discs, we have checked that this is not the cause behind the difference in alignment strength of the two populations.

Fig. A2 shows the average stellar and total satellite galaxy mass functions of our sample. Luminous satellites consist of haloes and subhaloes with at least one star particle, so they can have stellar masses as low as $\sim 2 \times 10^6\,\mathrm{M}_\odot$, which corresponds to the resolution limit of the EAGLE simulation. The same satellites have a typical total mass, $M_{\rm tot} \sim 1 \times 10^9\,\mathrm{M}_\odot$, which, since they are DM dominated, corresponds to ∼100 DM particles. For comparison, we also show the stellar mass function within a 3D distance of 300 kpc from MW and M31, which we take from the McConnachie (2012) compilation. We only show the MW and M31 satellites brighter than −8.8 in absolute V-band magnitude since these were the ones used in our study. Considering fainter satellites would change the observed mass functions only below a stellar mass of $5 \times 10^5\,\mathrm{M}_\odot$. While the EAGLE satellite mass function agrees with observations at high masses, it is systematically higher in the range $M_\star \lesssim 5 \times 10^6\,\mathrm{M}_\odot$, especially when compared to the MW. This is an outcome of selecting only haloes with 11 or more satellites, which biases our results towards a high satellite count.

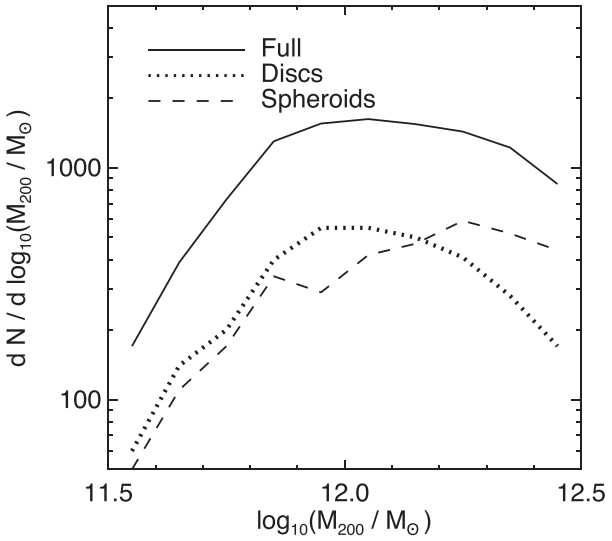

Figure A1. The number of haloes, N, as a function of halo mass for the sample of systems that met our selection criteria. Each of the disc and spheroid galaxy subsamples contains roughly a third of the full sample.

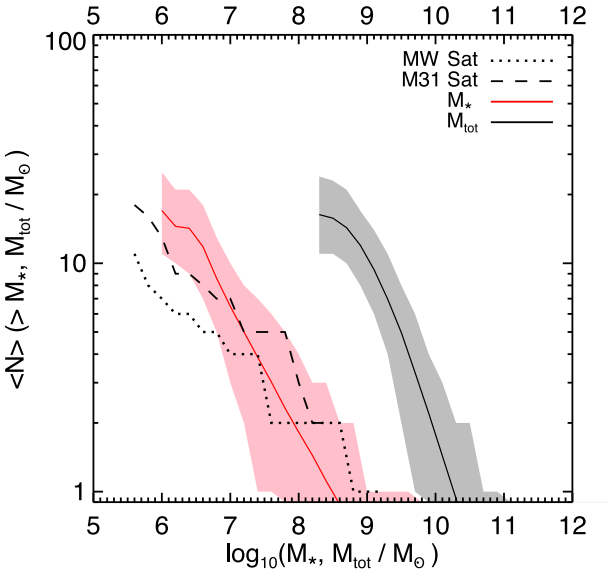

Figure A2. The mean number of luminous satellites per halo as a function of their stellar, $M_\star$, and total, $M_{\rm tot}$, masses. The shaded regions indicate the 10th and 90th percentiles scatter, while the solid lines indicate the mean value. The dotted and dashed lines show the observed stellar mass function within a distance of 300 kpc from the MW and the M31.

This paper has been typeset from a TEX/LATEX file prepared by the author.